




## RESEARCH ARTICLE

# Metabolic profiling of aortic stenosis and hypertrophic cardiomyopathy identifies mechanistic contrasts in substrate utilization

Nikhil Pal<sup>1,2</sup> | Animesh Acharjee<sup>3,4,5</sup>  | Zsuzsanna Ament<sup>3,4</sup>  | Tim Dent<sup>1</sup> |  
Arash Yavari<sup>1,2</sup> | Masliza Mahmood<sup>1</sup> | Rina Ariga<sup>1</sup> | James West<sup>3,4</sup> |  
Violetta Steeples<sup>6</sup> | Mark Cassar<sup>1</sup> | Neil J. Howell<sup>7</sup> | Helen Lockstone<sup>6</sup> |  
Kate Elliott<sup>6</sup> | Parisa Yavari<sup>1</sup> | William Briggs<sup>3</sup> | Michael Frenneaux<sup>8</sup> |  
Bernard Prendergast<sup>1</sup> | Jeremy S. Dwight<sup>1</sup> | Rajesh Kharbanda<sup>1</sup> | Hugh Watkins<sup>1</sup> |  
Houman Ashrafian<sup>1,2</sup>  | Julian L. Griffin<sup>3,4,9</sup> 

<sup>1</sup>Division of Cardiovascular Medicine, University of Oxford, John Radcliffe Hospital, Oxford, UK

<sup>2</sup>Department of Experimental Therapeutics, Radcliffe Department of Medicine, University of Oxford, John Radcliffe Hospital, Oxford, UK

<sup>3</sup>Department of Biochemistry, Cambridge Systems Biology Centre, University of Cambridge, Cambridge, UK

<sup>4</sup>MRC-Human Nutrition Research Unit, University of Cambridge, Cambridge, UK

<sup>5</sup>Institute of Cancer and Genomic Sciences, Centre for Computational Biology, University of Birmingham, Birmingham, UK

<sup>6</sup>Wellcome Trust Centre for Human Genetics (WTCHG), University of Oxford, Oxford, UK

<sup>7</sup>Department of Cardiothoracic Surgery, University Hospital Birmingham, Birmingham, UK

<sup>8</sup>Norwich Medical School, University of East Anglia, Bob Champion Research and Educational Building, Norwich, UK

<sup>9</sup>The Rowett Institute, University of Aberdeen, Aberdeen, UK

## Correspondence

Houman Ashrafian, Experimental Therapeutics, Radcliffe Department of Medicine, University of Oxford, John Radcliffe Hospital, Oxford OX3 9DU, UK.

Email: [houman.ashrafian@cardiov.ox.ac.uk](mailto:houman.ashrafian@cardiov.ox.ac.uk)

## Abstract

Aortic stenosis (AS) and hypertrophic cardiomyopathy (HCM) are distinct disorders leading to left ventricular hypertrophy (LVH), but whether cardiac metabolism substantially differs between these in humans remains to be elucidated. We undertook an invasive (aortic root, coronary sinus) metabolic profiling in patients with severe AS and HCM in comparison with

**Abbreviations:** AR, aortic root; AS, aortic stenosis; CPT-1, carnitine palmitoyltransferase 1; CS, coronary sinus; ECG, electrocardiogram; ECHO, transthoracic echocardiography; FAO, fatty acid oxidation; FFA, free fatty acid; FV, femoral vein; HCM, hypertrophic cardiomyopathy; HF, heart failure; LC, liquid chromatography; LV, Left ventricular; MS, mass spectrometry; PGC-1 $\alpha$ , PPAR $\gamma$  coactivator-1 $\alpha$ ; PLS-DA, partial least squares discriminant analysis; PPAR, peroxisome proliferation activated receptor; RF, random forest; ROC, receiver operator control; RXR $\alpha$ , retinoid X receptor  $\alpha$ ; UPLC, ultra-high performance chromatography; VIP, variable importance in projection.

Nikhil Pal, Animesh Acharjee, Zsuzsanna Ament, Houman Ashrafian, and Julian L. Griffin contributed equally to this study.

This is an open access article under the terms of the [Creative Commons Attribution](https://creativecommons.org/licenses/by/4.0/) License, which permits use, distribution and reproduction in any medium, provided the original work is properly cited.

© 2024 The Authors. *The FASEB Journal* published by Wiley Periodicals LLC on behalf of Federation of American Societies for Experimental Biology.

Julian L. Griffin, The Rowett Institute,  
University of Aberdeen, Aberdeen  
AB25 2ZD, UK.  
Email: [jules.griffin@abdn.ac.uk](mailto:jules.griffin@abdn.ac.uk)

### Funding information

UKRI | Medical Research Council (MRC), Grant/Award Number: MR/P011705/1, MC\_UP\_A090\_1006 and MR/S010483; British Heart Foundation (BHF); NIHR | NIHR Oxford Biomedical Research Centre (OxBR)

non-LVH controls to investigate cardiac fuel selection and metabolic remodeling. These patients were assessed under different physiological states (at rest, during stress induced by pacing). The identified changes in the metabolome were further validated by metabolomic and orthogonal transcriptomic analysis, in separately recruited patient cohorts. We identified a highly discriminant metabolomic signature in severe AS in all samples, regardless of sampling site, characterized by striking accumulation of long-chain acylcarnitines, intermediates of fatty acid transport across the inner mitochondrial membrane, and validated this in a separate cohort. Mechanistically, we identify a downregulation in the PPAR- $\alpha$  transcriptional network, including expression of genes regulating fatty acid oxidation (FAO). In silico modeling of  $\beta$ -oxidation demonstrated that flux could be inhibited by both the accumulation of fatty acids as a substrate for mitochondria and the accumulation of medium-chain carnitines which induce competitive inhibition of the acyl-CoA dehydrogenases. We present a comprehensive analysis of changes in the metabolic pathways (transcriptome to metabolome) in severe AS, and its comparison to HCM. Our results demonstrate a progressive impairment of  $\beta$ -oxidation from HCM to AS, particularly for FAO of long-chain fatty acids, and that the PPAR- $\alpha$  signaling network may be a specific metabolic therapeutic target in AS.

### KEYWORDS

cardiac gradient, cardiac metabolism, ischemic heart disease, metabolomics, precision medicine

## 1 | INTRODUCTION

The healthy heart primarily relies on fatty acid  $\beta$ -oxidation (FAO), utilizing circulating free fatty acids (FFA) or lipoprotein-derived triacylglycerols (50%–70% ATP requirements), but also consumes carbohydrates (glucose), lactate, branched-chain amino acids, and ketones.<sup>1</sup> This metabolic flexibility enables the heart to meet physiological workloads.

The balance between cellular energy metabolism and contractile performance is disrupted in cardiac disease. Individuals with advanced chronic heart failure (HF) consistently display reduced cardiac high-energy phosphates (with up to 30% lower absolute cardiac [ATP]),<sup>2</sup> and this is reproduced in animal HF models.<sup>3</sup> Myocardial phosphocreatine:ATP ratio, an index of cardiac bioenergetic state, correlates with HF severity and strongly predicts mortality.<sup>4</sup> Such observations highlight the energy-deplete state of the failing heart<sup>5</sup> and perturbations in cardiac intermediary energy metabolism.

Studies of the failing myocardium indicate substantial metabolic reconfiguration including: increased reactive oxygen species production,<sup>6</sup> substrate utilization switch from FFA to glucose,<sup>7</sup> FAO downregulation,<sup>8</sup> an

uncoupling between glucose uptake and oxidation,<sup>9</sup> impaired mitochondrial respiration<sup>10</sup> and decreased mitochondrial/cytosolic creatine kinase flux,<sup>11</sup> together with loss of metabolic flexibility to stress.<sup>12</sup> These are partly driven by nuclear receptor and transcriptional co-regulator signaling circuits orchestrating fuel selection and mitochondrial oxidative capacity, including peroxisome proliferator-activated receptor  $\alpha$  (PPAR $\alpha$ ),<sup>13</sup> a fatty-acid ligand binding master transcription factor promoting FAO; along with interacting regulators of oxidative metabolism retinoid X receptor  $\alpha$  (RXR $\alpha$ ),<sup>14</sup> estrogen-related receptor  $\alpha$  (ERR $\alpha$ ), and PPAR $\gamma$  coactivator-1 $\alpha$  (PGC-1 $\alpha$ ).<sup>15</sup> Such changes have been conceptualized as a return to a fetal metabolic program adapted to hypoxia, with preferential carbohydrate use and associated improvement in myocardial oxygen efficiency,<sup>16</sup> but whether these become maladaptive with HF progression remains unclear. Supporting a *causal* role for cardiac metabolic dysregulation, impaired FAO precedes systolic impairment in experimental models of left ventricular (LV) pressure overload<sup>17</sup>; conversely, relief of hemodynamic stress restores oxidative metabolism before functional and structural recovery.<sup>18</sup> Accordingly, therapies manipulating cardiac substrate

utilization have been trialed, including perhexiline,<sup>19</sup> etomoxir,<sup>20</sup> and trimetazidine,<sup>21</sup> with variable impact on energetics and/or symptoms, through blockade of carnitine palmitoyltransferase 1 (CPT-1), which catalyzes the rate-limiting step in mitochondrial  $\beta$ -oxidation.

In parallel with metabolic reconfiguration, a hallmark of the cardiac response to stress is structural remodeling, specifically left ventricular hypertrophy (LVH).<sup>22</sup> LVH can be primary in origin, exemplified by familial hypertrophic cardiomyopathy (HCM), or secondary to excessive hemodynamic loading (LV volume or pressure overload). Pressure overload-induced LVH, commonly resulting from aortic valvular stenosis (AS) or hypertension, is traditionally regarded as a compensatory mechanism normalizing systolic wall stress<sup>23</sup> which, if persistent paradigmatically transitions to frank HF. LVH is associated with reduced myocardial high-energy phosphate content<sup>24</sup> and consistently predicts adverse clinical outcomes including mortality and HF.<sup>25,26</sup> Inappropriately high LV mass is associated with higher cardiovascular risk in both HCM<sup>27</sup> and AS,<sup>28</sup> while LVH regression through hemodynamic unloading (e.g., antihypertensive therapy) lowers cardiovascular risk.<sup>29</sup> Morphologically, distinct LVH geometries have been identified which relate to cardiovascular risk,<sup>30</sup> but without parallel progress in defining specific metabolic endotypes, a prerequisite for precision therapeutics targeting metabolism. We reasoned that analysis of the metabolome—reflecting a convergence of multiple levels of biological organization and being functionally proximate to disease—in distinct LVH etiologies could address this shortfall to: (i) identify discriminant metabolic endotypes; (ii) provide disease-specific mechanistic insights; and (iii) generate hypotheses for translational testing.<sup>31</sup>

## 2 | METHODS

### 2.1 | Overall study design

#### 2.1.1 | Study design

We undertook a prospective single-center observational study at the John Radcliffe Hospital, Oxford, UK to characterize the metabolome from three groups of patients: (1) HCM, (2) AS with left ventricular hypertrophy, and (3) controls. Ethical approval was granted by the National Research Ethics Service (NRES) Committee South Central-C (number 13/SC/0155) and was monitored by the University of Oxford clinical trials and research governance department. All human studies conformed to the principles outlined in the Declaration of Helsinki.

The initial aim was to recruit an equal number ( $n = 35$ ) of participants to each of the three cohorts, forming a total of 105 participants (discovery cohort). The results from the discovery cohort were then validated in a set of peripheral samples collected from a separate cohort of patients (validation cohort). These metabolomic findings were subsequently validated using an orthogonal technology, by performing transcriptomic analysis of the genes regulating these metabolic pathways, in LV biopsy samples from a separate cohort of AS and control patients.

#### 2.1.2 | Recruitment

Participants were aged 18 years or above with a known diagnosis of AS or HCM and were undergoing angiography on the basis of prior determined clinical need. Controls were recruited as patients with clinically suspected coronary artery disease with normal systolic function, who were referred for diagnostic coronary angiography and in whom this revealed unobstructed coronary arteries. Patients underwent baseline phenotyping, including clinical history, routine blood test, electrocardiogram (ECG), and transthoracic echocardiography (ECHO). Patients with severely impaired LV systolic function or conduction abnormality on ECG were excluded.

For transcriptomic analysis, the LV biopsy samples (no specific region within LV) were collected from patients with severe AS ( $n = 36$ ) and controls (patients with ischemic heart disease and normal LV systolic function) undergoing cardiac surgery ( $n = 14$ ).

#### 2.1.3 | Procedure

Following informed consent, patients underwent cardiac catheterization. Following coronary angiography, plasma samples were collected at baseline and following right ventricular endocardial pacing from femoral vein (FV), coronary sinus (CS), and aortic root (AR). Pacing was commenced at 100 beats per minute for 60s and then incrementally increased every minute to a maximum of 140 beats per minute. Pacing was undertaken for a total duration of 3 min or stopped sooner if patient developed chest pain or ECG changes. In the validation cohort, peripheral blood samples were obtained from a vein in the arm.

The blood samples were placed on ice and centrifuged at 3500 rpm at 4°C for 15 min. The supernatant was double aliquoted into Eppendorf tubes with re-centrifuged at 5000 rpm for 5 min in between, then stored at  $-80^{\circ}\text{C}$ .

## 2.2 | Carnitine and aqueous metabolite analysis

HPLC grade solvents were obtained from Sigma Aldrich (Gillingham, Dorset, UK). All standards for optimization and quantitation were obtained from Sigma Aldrich with the exception of the internal standards, U-<sup>13</sup>C, <sup>15</sup>N-glutamine, D<sub>10</sub>-Leucine, D<sub>8</sub>-Phenylalanine, D<sub>8</sub>-Valine, U-<sup>13</sup>C, <sup>15</sup>N-Proline which were acquired from Cambridge Isotope Laboratories (Andover, MA, USA).

### 2.2.1 | Aqueous metabolite analysis

Samples were aliquoted (25- $\mu$ L blood plasma) to 96-well plates and proteins were precipitated using 400  $\mu$ L MeOH containing a mixture of five internal standards at 2.5  $\mu$ M. The precipitated samples were placed on a plate shaker for 5 min at 1000 rpm, and using a liquid handling robot (Viaflo 96, Integra Biosciences, Nottingham, UK) transferred onto 96-well 0.66 mm glass fiber polystyrene filter plates (Corning Inc., NY, USA). Samples were filtered and dried. Samples were re-constituted in 100  $\mu$ L of water containing 10-mM ammonium acetate and transferred to clean glass-coated 200- $\mu$ L 96-well plates. Two microliters of the sample was injected.

Chromatographic analyses were performed using a Dionex UltiMate 3000 system (Thermo Scientific, Hemel Hempstead, UK), with an ACE C18-PFP 3  $\mu$ m column (2.1  $\times$  150 mm) (Advanced Chromatography Technologies Ltd., Aberdeen, UK) coupled to a TSQ Quantiva Triple Quadrupole Mass Spectrometer (Thermo Scientific, Hemel Hempstead, UK) as described previously.<sup>32</sup> The mobile phase gradient was run at 0.5 mL/min using water (mobile phase A) and acetonitrile (mobile phase B). The gradient started at 100% A and increased to 60% B from 1.6 to 4.5 min. Data were acquired in both positive and negative ionization modes using a capillary spray voltage of 3.5 and 2.5 kV, respectively. The ion transfer tube was set to operate at 350°C whilst the vaporizer temperature was set to 400°C.

### 2.2.2 | Acylcarnitine analysis

Acyl-carnitines were measured according to the method described by Roberts et al.<sup>33</sup> Briefly, 100- $\mu$ L internal standard solution mix (1.63  $\mu$ M D<sub>9</sub>-free carnitine, 0.3  $\mu$ M D<sub>3</sub>-acetyl carnitine, 0.06  $\mu$ M D<sub>3</sub>-propionyl-carnitine, 0.06  $\mu$ M D<sub>3</sub>-butyryl-carnitine, 0.06  $\mu$ M D<sub>9</sub>-isovaleryl-ketocarnitine, 0.06  $\mu$ M D<sub>3</sub>-octanoyl-carnitine, 0.06  $\mu$ M D<sub>9</sub>-myristoyl-carnitine, and 0.12  $\mu$ M D<sub>3</sub>-palmitoyl-carnitine; Cambridge Isotope Laboratories, Andover, USA) was added to 40  $\mu$ L of the organic fraction of the methanol: chloroform extraction,

dried down under nitrogen, and derivatized with 100  $\mu$ L of 3 M butanolic-HCl (Sigma-Aldrich, Louis, Missouri, USA). Samples were evaporated under nitrogen, reconstituted, and sonicated in 4:1 acetonitrile: 0.1% formic acid in water.

Samples were analyzed using an AB Sciex 5500 QTRAP mass spectrometer (AB Sciex, Warrington, UK) coupled to an Acquity UPLC system. Mobile phase A consisted of 0.1% formic acid in water, while mobile phase B was acetonitrile. Two microliters of each sample was injected onto a Synergi Polar RP phenyl ether column (100 mm  $\times$  2.1 mm, 2.5  $\mu$ m; Phenomenex, Macclesfield, UK). The analytical gradient started at 30% B, followed by a linear increase to 100% B over 3 min. The gradient was then held at 100% B for 5 min, after which it was returned to the re-equilibration level of 30% B. A flow rate of 0.5 mL/min was used. Data were normalized against wet tissue weight and to the intensity of the internal standard. A complete list of metabolites is provided within the supplementary data (Supplementary Table S10).

### 2.2.3 | Statistical analysis and variable selection of the metabolomic data

We used two multivariate methods to both maximize separations and identify which metabolites are most important for these discriminations: partial least squares discriminant analysis (PLS-DA) and Random Forest (RF). As one of the primary objectives was to select the most important metabolites from the metabolites measured, a two-stage process was used. PLS-DA is a linear projection method, and all metabolites are assumed to be combined in a linear manner to maximize discrimination. In PLS-DA, the Variable Importance in Projection (VIP) scores were used to estimate the importance of each variable in the projection. RF does not assume any linearity, uses the sum of piecewise functions, and is able to discover more complex dependencies and produce a more discrete set of metabolites.

In RF, we used a backward elimination process to select the best metabolites which resulted in good accuracy in terms of discrimination. RF constructs a predictive model for the response using all predictors and quantifies the importance of each carnitine and aqueous metabolites, in explaining the misclassification error. We used a variable selection procedure to select the optimum number of metabolites and using those selected metabolites, RFs were iteratively fitted, so that they yielded the smallest out-of-bag error rates. We further compared multivariate receiver operator control (ROC) curves to study how the number of selected variables impacts ROC performance.

Multivariate data analysis using PCA and PLS-DA was performed in Simca 14.0 (Umetrics, Umeå, Sweden). RF



classification of the classes on carnitine and aqueous metabolites and selection of carnitines and aqueous metabolites was conducted using the “randomForest” and “varSelRF”<sup>34</sup> package of R statistical software (<https://www.r-project.org/>).

## 2.3 | Transcriptomic analysis

Gene expression arrays: Total RNA was extracted from snap-frozen and pulverized heart tissue using the RNeasy Mini Kit (Qiagen, UK) following the manufacturer’s recommendations. Subsequent steps of cDNA synthesis, hybridization, quality control, data normalization, and analysis were undertaken by the Genomics and Bioinformatics Core Facilities, Wellcome Trust Centre for Human Genetics, Oxford. Illumina BeadChip microarrays (human WG-6V2) were used according to the manufacturer’s protocols.

Raw intensity data were imported into the R statistical software (<http://www.R-project.org>) for further processing and analysis using BioConductor packages. Raw signal intensities were background corrected prior to being transformed and normalized. A range of quality control checks was made on the data and it was filtered to remove genes not detected above background levels (detection score <0.95) in at least three samples, resulting in a final dataset of 19205 genes and 30 samples (17 AS patients and 13 Controls).

Statistical analysis to identify differential gene expression was performed with the Linear Models for Microarray Analysis (limma) package.<sup>35</sup> Raw p-values were corrected for multiple testing using the false discovery rate (FDR) controlling procedure of Benjamini and Hochberg.

## 2.4 | In silico modeling of $\beta$ -oxidation

The model for human  $\beta$ -oxidation with competitive inhibition<sup>36,37</sup> was used within COPASI (<http://copasi.org/>). The impact of raising concentrations of palmitoyl-CoA in the cytosol and C14:0-carnitine in the mitochondria was investigated by raising fixed concentrations of both metabolites and performing a time course simulation across 800 iterations and 50 min to achieve model stability.

# 3 | RESULTS

## 3.1 | A targeted in vivo metabolomics strategy to probe human myocardial metabolism at baseline and during increased workload

To obtain a systematic quantitative assessment of cardiac metabolism in vivo in AS versus HCM populations, we

undertook targeted plasma metabolic profiling using liquid chromatography-tandem mass spectrometry (LC-MS/MS) to provide a comprehensive snapshot of substrate selection and metabolism (Figure 1A). These patient groups were compared to a group that had no valvular heart disease or cardiomyopathy, and following an angiogram for suspected coronary artery disease, which turned out to be negative, were defined as a group free of macrovascular cardiovascular disease. These were referred to as the control group although microvascular ischemia could not be excluded.<sup>38,39</sup> We focused on FAO, inferred from levels of acylcarnitine species, as well as intermediates from glycolysis, TCA cycle, amino acid, ketone, and 1-carbon metabolism. To analyze myocardial substrate utilization, we evaluated arteriovenous (AV) metabolite extraction by paired sampling of blood from the aortic root (AR, reflecting myocardial arterial blood supply) and coronary sinus (CS, representing cardiac venous effluent). Simultaneously samples from femoral venous (FV) blood to assess the ability of the peripheral metabolome to reflect myocardial biochemical alterations, as described for some metabolites.<sup>40</sup> We further explored the ability of selectively increasing myocardial work to impact the metabolomic phenotype and refine metabolomic signature by repeating sampling after right ventricular pacing.

This protocol was applied to a discovery cohort of AS ( $n=36$ ), HCM ( $n=35$ ), and control ( $n=38$ , individuals undergoing elective cardiac catheterization for suspected coronary artery disease) patients. Reflecting its natural history, AS subjects were older than HCM or control groups (mean  $80 \pm 7$  years vs.  $62 \pm 10$  or  $63 \pm 10$ , respectively), and had a higher incidence of hypertension and thus antihypertensive use (Table 1 and Supplementary Tables S1 and S2). Notably, on transthoracic echocardiography, all three groups showed evidence of left ventricular hypertrophy, although the extent was substantially less in the control group than in either the AS or HCM groups.

## 3.2 | Trans-myocardial arteriovenous extraction differences in LVH versus control

The trans-myocardial AV gradient of selected key carbon substrates (glucose, lactate, glutamate, and alanine) was first measured and the results from this were consistent with their previously reported role in cardiac metabolism at rest and during stress (Supplementary Figure S1).<sup>41,42</sup>

We next extended our analysis of trans-myocardial AV gradient to the complete metabolite profile for the cohort at baseline (Supplementary Table S3) and during pacing (Supplementary Table S4). This revealed significant cardiac extraction of glutamate, 2-oxo-isovalerate,

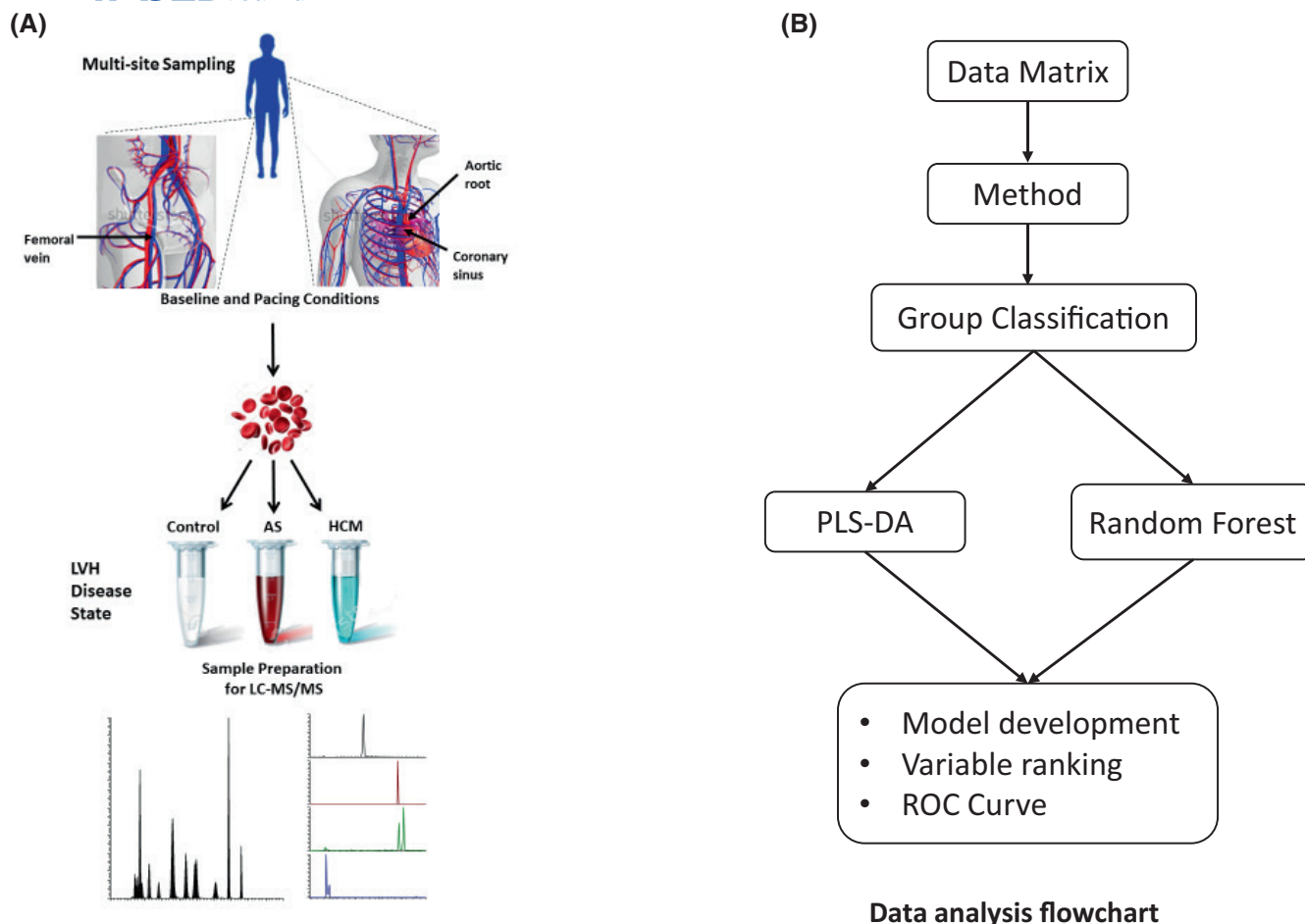


**FIGURE 1** Illustration of the workflow for the study. (A) This details the collection of blood samples from multiple sites in the human body and processing using mass spectrometry platforms (B) Overview of multivariate statistics used in the analysis of the data.

2-oxo-3-methylvalerate, 2-oxo-isocaproate, and pyruvate, but elution of succinate, in controls and AS at baseline. This pattern was largely recapitulated with pacing, with additional extraction of  $\beta$ -aminoisobutyric acid (BAIBA)<sup>43</sup> in AS. In the HCM cohort, we found net extraction of glutamate and elution of succinate, regardless of pacing. Notably, compared to controls, both LVH cohorts displayed reduced (by  $\sim 2/3$ ) AV extraction of glutamate—a key anaplerotic substrate contributing to cellular oxidative capacity.

We next performed PLS-DA on the trans-myocardial arteriovenous extraction differences to examine whether disease could be discriminated. However, the models produced for all three groups, and individual two-group comparison models were poor in terms of discrimination, so we next considered the metabolic profiles of the individual samples from different sites of collection.

### 3.3 | Distinct metabolic profiles discriminate between AS and HCM

The differences between cohorts across the three collection sites were next analyzed (Figure 1B). Models

were built to determine the most discriminating metabolites using individual collection sites separately and then in combination. An initial PLS-DA comparison of the three groups using the combined baseline and pacing samples from all three-collection sites generated a robust discriminating model, suggesting that disease status had more influence on the dataset rather than site of collection or pacing status (Figure 2A,B). An improved PLS-DA model was generated by comparing AS versus HCM and control combined as a single group (Figure 2C,D). This separation was driven by increases in C14-OH and C18-OH acylcarnitines, and aconitate, and a decrease in  $\alpha$ -ketoisocaproate, in the AS cohort. Similar results were obtained whether using metabolite levels from baseline or pacing samples separately or in combination; accordingly, further comparisons were made using the baseline samples only.

Next, a pair-wise comparison of the three groups using combined samples from all three sites was performed. This generated robust models discriminating: HCM versus control (Figure 3A); AS versus control (Figure 3B); and AS versus HCM (Figure 3C). All models passed the random permutation analysis and model misclassification,

**TABLE 1** Details of the clinical and demographic characteristics of the controls, aortic stenosis (AS), and hypertrophic cardiomyopathy (HCM) cohorts.

	Controls (n = 38)	Aortic stenosis (n = 36)	HCM (n = 35)	p value
Age (years)	63 ± 10	80 ± 7	62 ± 10	<.0001
Men, n %	79	53	71	.04
BMI (kg/m <sup>2</sup> )	26.1 (23.7–28.5)	28.1 (27.2–30.8)	27.5 (25.9–31.7)	.06
NYHA I	14 (36%)	3 (8%)	6 (17%)	.008
NYHA II	18 (47%)	19 (53%)	26 (74%)	.05
NYHA III	6 (16%)	11 (31%)	3 (9%)	.05
NYHA IV	0	3 (8%)	0	
LVEF, n%	61 ± 10	56 ± 12	66 ± 11	.004
PMH, n%				
Hypertension	50	75	40	.009
Diabetes	16	25	11	.3
Dyslipidemia	53	75	54	.09
COPD/Asthma	13	14	14	.9
IHD	37	25	3	.002
Family History of IHD	61	44	69	.1
Medications, n %				
Aspirin	68	42	57	.07
Clopidogrel	16	3	17	.1
ACE-I/ARB-II	47	75	14	<.0001
Beta-blockers	40	47	49	.7
Statin	66	61	46	.2
Calcium blockers	24	28	40	.3
Diuretics	16	72	11	<.0001
OHA	8	19	9	.2
Insulin	11	3	0	.08

Note: Differences between the cohorts were examined statistically using ANOVA with Bonferroni's post-test for multiple comparisons. Statistical significance was defined as a  $p < .05$ . Values are mean ± SD, percentages, or median (quartiles 1 to 3).

Abbreviations: ACE, angiotensin-converting enzyme inhibitors; ARB, angiotensin-receptor antagonist-II; BMI, body mass index; IHD, ischemic heart disease; OHA, oral hypoglycemic agent; PMH, past medical history.

performed to assess their validity and goodness of fit (Figure 3D and Supplementary Figure S2). AS was clearly discriminated from both HCM and control cohorts: 94% correct across 362 samples and 90% correct across 370 samples, respectively.

Variable Importance in Projection (VIP) scores were then used to rank the relative discriminatory value of metabolites responsible for the classification of AS versus control (37 metabolites with a VIP score >1), HCM versus control (31 metabolites), and AS versus HCM (41 metabolites) comparisons (Supplementary Figure S3). Of these, the following metabolites were common to all three comparisons: isocitrate, proline, valine, carnitine, C2, C10, C14:1, C14-OH, C16, C16-OH, and C18-OH, while some metabolites were disease specific: AS versus control (asparagine, carnitine, ornithine, and C6-DC and C6 acylcarnitines) and HCM versus control (alanine, betaine,

leucine, methionine, and C18:2-OH, C16:1-OH, and C16:2 acylcarnitines).

PLS-DA analysis examining pairwise comparisons from CS, FV, and AR samples separately was then performed. The most discriminating models were built using the CS samples, where robust models discriminating AS from control (Figure 3E) and AS from HCM (Figure 3G) were built. The model discriminating AS from control passed the random permutation test, CV-ANOVA ( $p = 1.2 \times 10^{-5}$ ) and produced ROC with AUC = 0.95 (Figure 3H). This classification was driven, in part, by increases in cystine, BAIBA, and S-adenosyl methionine, and decreases in C8-DC acylcarnitine, asparagine, and  $\alpha$ -ketoisocaproate in the AS cohort (Figure 3F). The discrimination between AS and HCM cohorts was driven by greater concentrations of malate and C14-OH, C20:1, and C12 acylcarnitines, and lower concentration of  $\alpha$ -ketoisocaproate, uridine, and

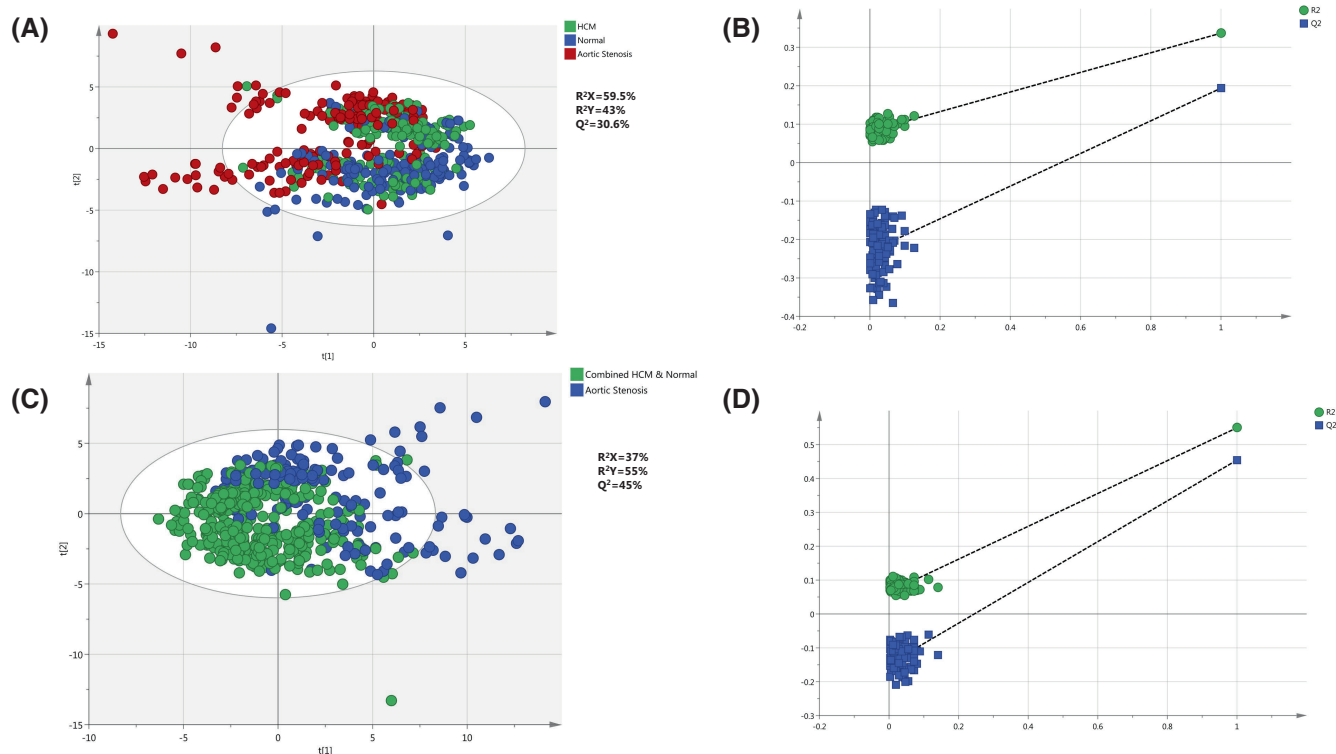


**FIGURE 2** Score and validation plots showing comparison of aortic stenosis, HCM, and control cohorts. (A) Score plot comparing all three cohorts. A robust model was built discriminating all three cohorts using PLS-DA ( $R^2X=59.5\%$ ,  $R^2Y=43\%$ ,  $Q^2=30.6\%$ ). (B) Validation plot comparing all three cohorts, a robust model was built discriminating all three cohorts using PLS-DA. (C) Score plot comparing the aortic stenosis cohort with the combined samples from HCM and control cohorts. A robust model was built using PLS-DA ( $R^2X=37\%$ ,  $R^2Y=55\%$ ,  $Q^2=45\%$ ). (D) Validation plot comparing the aortic stenosis cohort with the combined samples from the HCM and control cohorts. The main discrimination was between aortic stenosis samples and the other two cohorts combined together. Multivariate plots are based on 38 individuals in the control group, 36 in the aortic stenosis group, and 35 in the hypertrophic cardiomyopathy group. Score plots include blood plasma samples from the coronary sinus, aortic root, and femoral vein.

histidine in the AS cohort. Similar analyses were also performed on the FV and AR samples (Supplementary Figures S4–S7), which produced similar, albeit less robust models as compared to the CS.

The significant age difference between subjects in the AS group and the other two groups was investigated by stratifying for age, to investigate whether this had an impact on the multivariate models constructed. Subjects over the age of 70 years were selected, and samples from all three collection sites collected both at baseline and pacing were included (Supplementary Figure S8A). A robust model discriminating AS and control cohorts was generated (Supplementary Figure S8B), which was validated using random permutation analysis (Supplementary Figure S8C). Also, several of the most discriminating metabolites were common between models built pre- and post-age stratification (Supplementary Figure S8D). Similarly, models discriminating control versus HCM and AS versus HCM cohorts for subjects over 70 years of age were also assembled.

We also investigated whether drug treatment had an impact on the metabolome either stratified for disease group or regardless of disease status according to the data in Table 1. No multivariate model passed cross-validation for these drug treatments demonstrating that any effects associated with a given pharmaceutical intervention were minor in comparison with either disease status, age, or sex where robust models could be built.

To further validate the performance of the pairwise classification models, we used the selected metabolites to build RF models and generated ROC curves (Supplementary Figure S9). This analysis demonstrated good predictive ability of the selected metabolites to differentiate AS from the control cohort (Figure 4A–C), associated with accumulation of long-chain acyl-carnitines in the AS cohort, suggesting a downregulation of FAO. On a three-way analysis between cohorts, the long-chain acylcarnitines C16:1 and C18-OH were present in incrementally higher concentrations (significantly different between the pairs) between the control, HCM, and AS



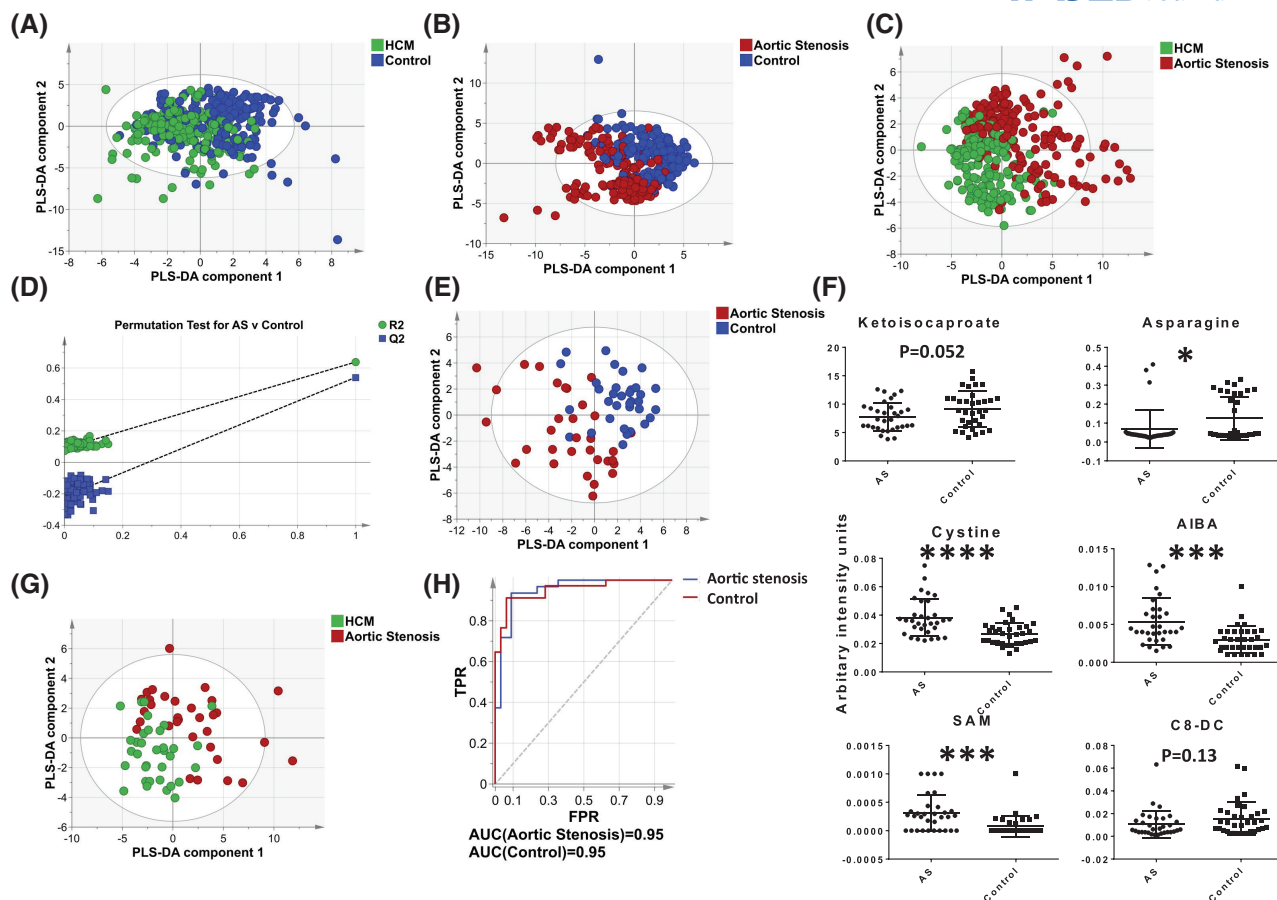


**FIGURE 3** Multivariate pairwise-analysis of patient groups. (A) PLS-DA comparison between the HCM and control groups using blood samples from all three sampling sites (CS, AR, and FV) ( $R^2X=36\%$ ,  $R^2Y=41\%$ ,  $Q^2=18\%$ ). (B) PLS-DA comparison between the AS and control groups using blood samples from all three sampling sites (CS, AR, and FV) ( $R^2X=38\%$ ,  $R^2Y=64\%$ ,  $Q^2=54\%$ ). (C) PLS-DA comparison between the HCM and AS groups using blood samples from all three sampling sites (CS, AR, and FV) ( $R^2X=44\%$ ,  $R^2Y=70\%$ ,  $Q^2=53\%$ ). (D) Random permutation test of the model validity for the model in B. (E) PLS-DA comparison between the control and AS groups using blood samples from the CS ( $R^2X=30\%$ ,  $R^2Y=59\%$ ,  $Q^2=37\%$ ). (F) Box-whisker plots of key metabolites that are discriminatory between the AS and control groups for the model in e. (G) PLS-DA comparison between the HCM and AS groups using blood samples from the CS ( $R^2X=29\%$ ,  $R^2Y=47\%$ ;  $Q^2=18\%$ ). (H) ROC analysis of the predictive capability of the model in E discriminating between AS and control groups. Multivariate plots are based on 38 individuals in the control group, 36 in the aortic stenosis group, and 35 in the hypertrophic cardiomyopathy group. Score plots include blood plasma samples from the coronary sinus, aortic root, and femoral vein for plots A–C.

cohorts, in the FV and AR collection sites (controls < HCM < AS).

Results from the discovery cohort comparing the AS and control cohorts were validated by analyzing samples from the validation cohort. Compared to the discovery cohort, subjects with AS in the validation cohort were younger (71 vs. 81 years,  $p < .0001$ ), while controls in both cohorts were well matched for age (62 vs. 61 years,  $p = .09$ ). All subjects had normal LV ejection fraction and the majority were males (Supplementary Table S5). Exploratory principal component analysis (PCA) on all samples (AS and control combined) displayed clear separation between the discovery and validation cohorts (Figure 4D) which was associated with increases in alpha-amino adipic acid and C2 carnitine in the

validation cohort and increases in C12, C10:2, C8-OH, C10:1, and C5-DC carnitine species the original cohort. These metabolites were consistently changed for both cohorts (i.e., in both the control and AS groups) and may represent consistent changes associated with sample handling or storage between the two cohorts. However, application of the multivariate model derived from the discovery cohort to the validation cohort discriminated AS and control cohorts (AUC = 0.76, Figure 4E).

We examined the original discovery dataset using ANOVA with Tukey's multiple comparison post-tests to examine the alterations in specific acyl-carnitine species as measured in blood plasma collected from the coronary sinus. Carnitine ( $p = .008$  for ANOVA), C2-carnitine ( $p = .014$ ), C10-carnitine ( $p = .005$ ), C14-OH carnitine

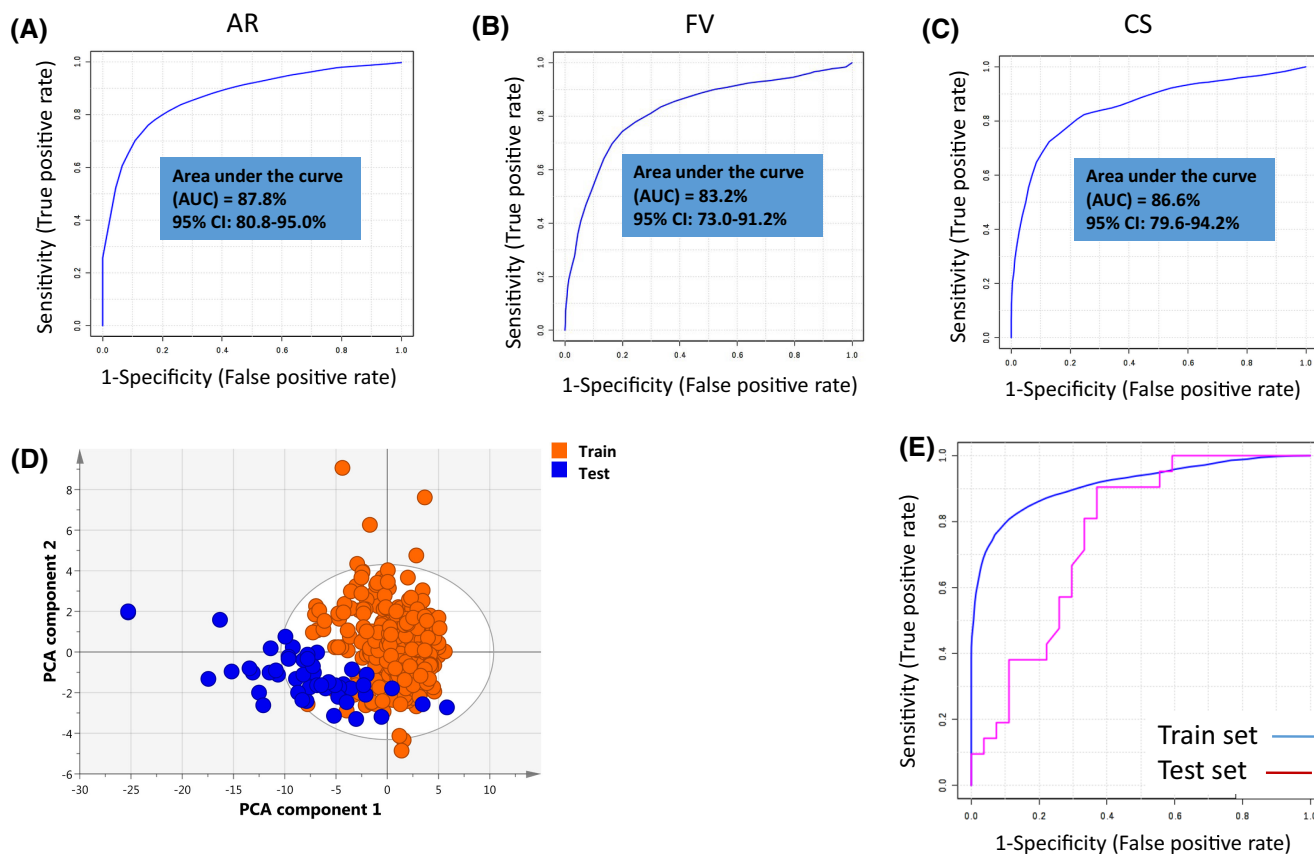


**FIGURE 4** Multivariate and ROC curve analysis comparing the discovery and validation cohorts. (A–C): ROC curve analysis comparing control and aortic stenosis cohorts from the discovery group. The analysis is performed individually for samples collected from the three sites: AR (Aortic root), FV (Femoral vein), and CS (Coronary sinus). (D) PCA score plot of AS and control cohorts from the discovery and validation groups (for all metabolites combined). (E) ROC curves analysis comparing the FV samples from the discovery group (blue line) to the peripheral vein samples from the validation group (purple line). Discovery group consisted of 38 individuals in the control group and 36 in the aortic stenosis group. The validation group consisted of 23 individuals in the control group and 27 in the aortic stenosis group.

( $p=.0009$ ), C16:1 carnitine ( $p=.0048$ ), C16:0-OH carnitine ( $p=.0002$ ), C18-OH carnitine ( $p=.0044$ ), and total acyl-carnitines ( $p=.0002$ ) all increased from control > HCM > AS (Figure 5).

### 3.4 | The cardiac transcriptomic profile of severe aortic stenosis

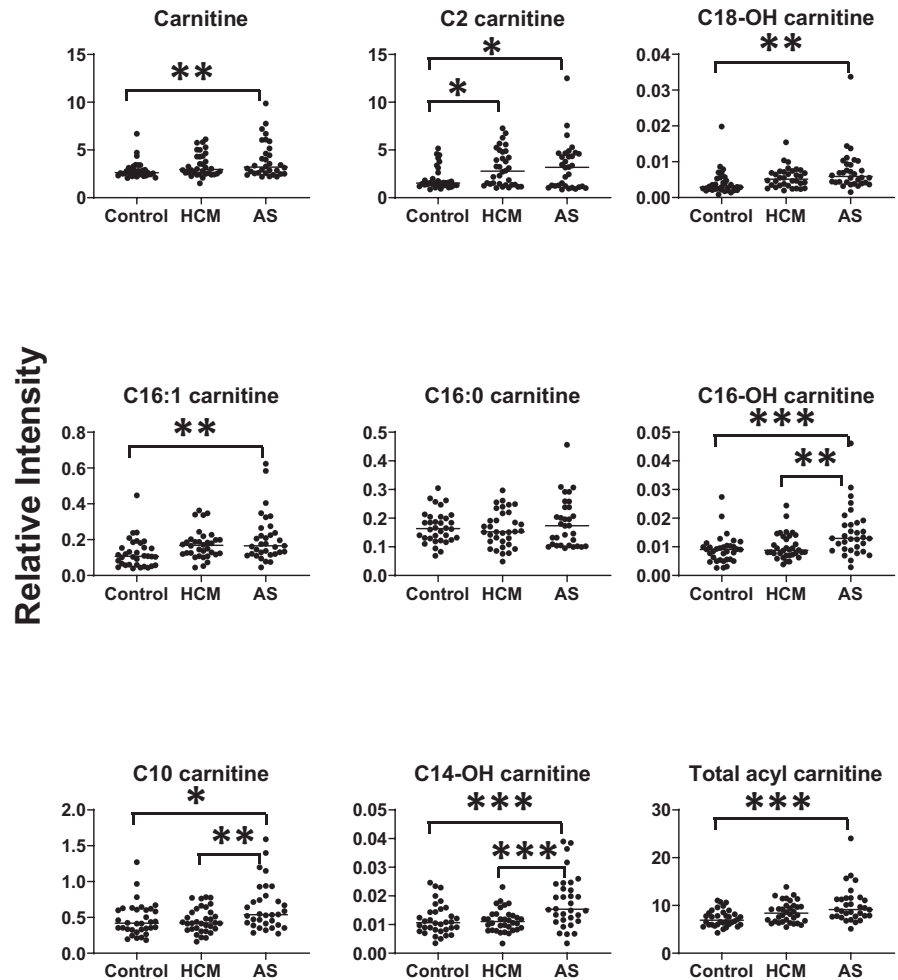
To gain a more integrated understanding of the cellular consequences of AS-induced LVH and the mechanistic relevance of our plasma-based metabolomic findings, we used an orthogonal approach to examine the cardiac transcriptome in AS. We used whole-genome microarrays (Illumina) to profile intra-operative LV biopsies from 36 individuals with severe AS undergoing aortic valve replacement (AVR) in comparison with 14 control subjects (patients with coronary artery disease, normal LV systolic function, and no significant aortic valve disease) undergoing coronary artery bypass grafting for ischemic heart disease. The majority of patients in both groups were

male, with no difference in age (71 vs. 68 years,  $p=.84$ ) (Supplementary Table S6).

Differentially expressed genes were identified using the Linear Models for Microarray Analysis (limma) package.<sup>44</sup> Of 19 205 genes that passed filtering criteria, 8415 genes were significantly altered in AS at a false discovery rate (FDR) of 5%. Pathway enrichment analysis was performed using Ingenuity Pathway Analysis (IPA) on a subset of the differentially expressed genes (3656 had adjusted  $p < .001$ ). Of 453 canonical pathways, 158 were significantly enriched ( $p < .05$ ) for genes found altered in AS. These included some important metabolic pathways such as adipogenesis (ranked 2,  $p = 1.6 \times 10^{-8}$ ), PPAR signaling (ranked 48,  $p = 2.4 \times 10^{-3}$ ), and PPAR $\alpha$ /RXR $\alpha$  activation (ranked 51,  $p = 2.8 \times 10^{-3}$ ) (Supplementary Table S7 and Figure S10).

Consistent with the notion of energetic privation in LVH, we observed significant changes in the expression of genes encoding subunits of the cellular energy sensor AMP-activated protein kinase (AMPK) in AS including downregulation of protein kinase, AMP-activated,

**FIGURE 5** Summary of ANOVA analysis followed by Tukey's post-test to examine changes in acyl-carnitines in the discovery dataset as measured in blood plasma taken from the coronary sinus. All displayed acyl-carnitines were significant with respect to ANOVA apart from C16:0-carnitine. Key: results from Tukey's post-tests following a positive ANOVA test: \* $p < .05$ , \*\* $p < .01$ , \*\*\* $p < .001$ . Plots are based on 38 individuals in the control group, 36 in the aortic stenosis group, and 35 in the hypertrophic cardiomyopathy group.



beta 1 non-catalytic subunit (*PRKAB1*) and protein kinase, AMP-activated, gamma 1 non-catalytic subunit (*PRKAG1*) and upregulation of protein kinase, AMP-activated, gamma 2 non-catalytic subunit (*PRKAG2*), and protein kinase, AMP-activated, alpha 1 catalytic subunit (*PRKAA1*) (Supplementary Table S8). Supporting the potential functional relevance of these findings, mice deficient in  $\alpha 2$  AMPK develop more marked LVH and poorer contractile performance in response to pressure overload.<sup>45</sup>

We also found differential expression in genes regulating different steps of FAO, including decreased expression of solute carrier family 27 (fatty acid transporter), member 5 (*SLC27A5*), and fatty acid binding protein 6 (*FABP6*) genes involved in the transport of FA across the sarcolemmal membrane, and increased expression of acyl-CoA synthetase long-chain family member 3 (*ACSL3*), which encodes proteins that convert long-chain FA into their acyl-CoA derivatives via thio-esterification.

Further investigation of genes involved in peroxisomal  $\beta$ -oxidation revealed increased expression of ATP binding

cassette subfamily D member 3 (*ABCD3*), acyl-CoA oxidase 1, palmitoyl (*ACOX1*), enoyl-CoA hydratase/3-hydroxyacyl CoA dehydrogenase (*EHHADH*), and hydroxysteroid (17-beta) dehydrogenase 4 (*HSD17B4*) genes. This was, thus, indicative of increased FAO via the peroxisomal  $\beta$ -oxidation route.

There was a decrease in expression of genes from the acyl-CoA thioesterase family (*ACOT1*, *ACOT4*, *ACOT7*, and *ACOT8*), encoding proteins that hydrolyze the CoA thioester of FA. These FFA can then be transported out of the peroxisomes into the mitochondria for further oxidation. There was increased expression of *CROT*, encoding a protein which catalyzes the conversion of acyl-CoA to acylcarnitine, allowing transfer of the acylcarnitines from peroxisome/cytosol to mitochondria.

Reviewing genes involved in mitochondrial  $\beta$ -oxidation, we found decreased expression of genes involved in transport of acylcarnitines across the mitochondrial membrane (carnitine palmitoyltransferase 1A (*CPT1A*), carnitine palmitoyltransferase 2 (*CPT2*), and solute carrier family 25 (Carnitine/Acylcarnitine Translocase), member 20 (*SLC25A20*)). There was also

decreased expression of acyl-CoA dehydrogenase family member 8 (*ACAD8*) and hydroxysteroid (17-beta) dehydrogenase 10 (*HSD17B10*).

Several genes involved with microsomal FAO were also found significantly downregulated: cytochrome P450, family 4, subfamily B, polypeptide 1 (*CYP4B1*), cytochrome P450, family 27, subfamily A, polypeptide 1 (*CYP27A1*) and cytochrome P450, family 4, subfamily X, member 1 (*CYP4X1*). Thus, there was a possible reduction in the amount of FAO via the mitochondrial and microsomal routes.

We identified further evidence of remodeled myocardial lipid metabolism in AS, with downregulation in multiple genes encoding proteins regulating lipid biosynthesis including fatty acid elongase 1 (*ELOVL1*) catalyzing long-chain fatty acid elongation at the endoplasmic reticulum; diacylglycerol O-acyltransferase 2 (*DGAT2*) that catalyzes triacylglycerol synthesis; 1-acylglycerol-3-phosphate O-acyltransferase 5

(*AGPAT5*) and 1-acylglycerol-3-phosphate O-acyltransferase 7 (*AGPAT7*), both involved in phospholipid synthesis. Despite the reduction in multiple PPAR $\alpha$  target genes, we observed a modest upregulation in the expression of *PPARA* itself in AS patients (log<sub>2</sub>-fold change 0.43,  $p = .0009$ ) which along with the increased expression of peroxisomal  $\beta$ -oxidation suggests that PPAR $\alpha$  signaling is partially disrupted.

We also identified significant changes in genes encoding enzymes which regulate glycolysis, including upregulation of 6-phosphofructo-2-kinase/fructose-2,6-biphosphatase 2 (*PFKFB2*), and downregulation of glucose 6 phosphatase, catalytic, 3 (*G6PC3*), phosphoenolpyruvate carboxykinase 2 (*PCK2*), pyruvate dehydrogenase kinase, isozyme 1 & 2 (*PDK & PDK2*). Aconitase 2 (*ACO2*), the mitochondrial enzyme catalyzing inter-conversion of citrate to isocitrate during the TCA cycle, was downregulated.

This analysis of the transcriptome reveals multiple changes in the myocardial energy sensing and generation

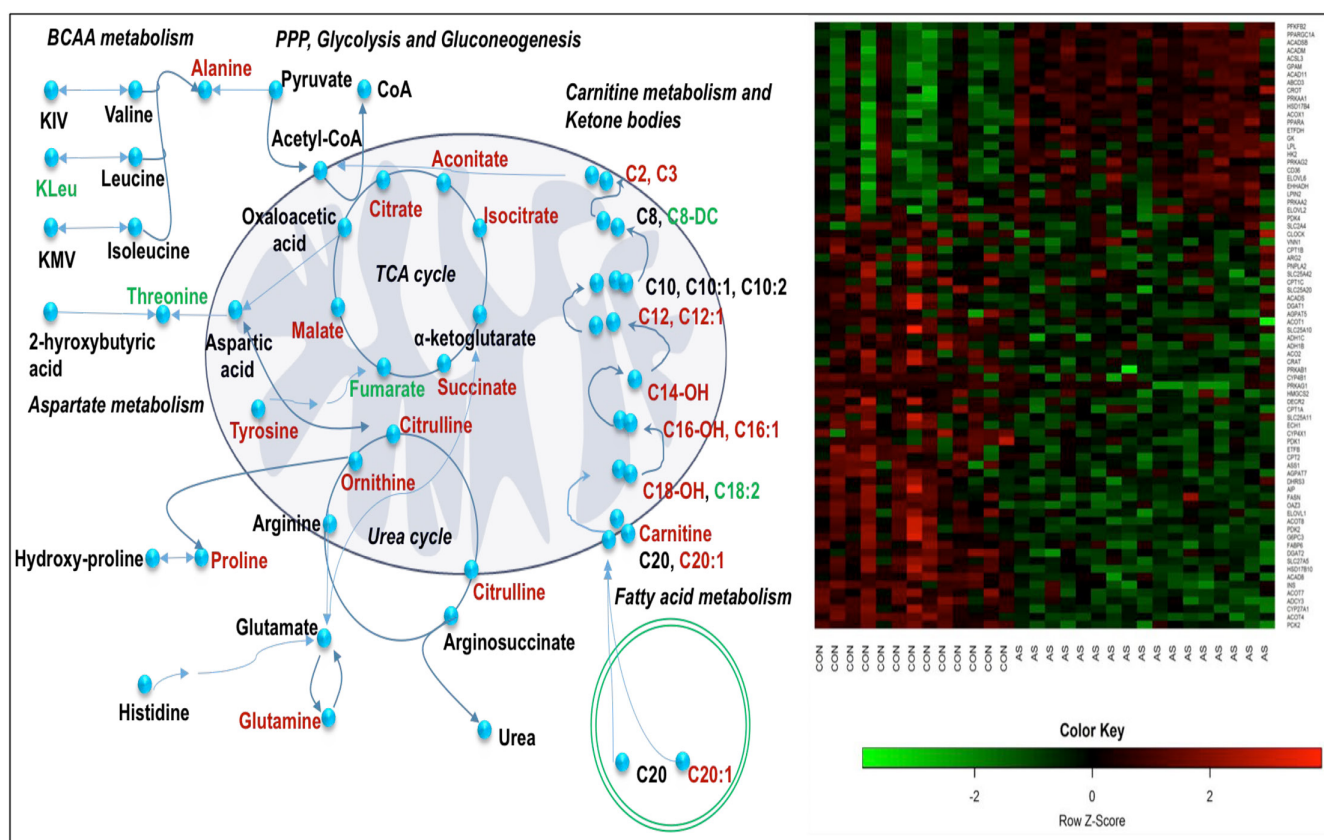


**FIGURE 6** Overview map of impacted metabolic pathways and metabolite changes, along with the heat map of associated metabolism-related genes depicting their expression profiles, in aortic stenosis (AS) compared to controls. The concentration of the metabolite change was labeled green for a decreased concentration, red for increased concentration, and black for no change in concentration. The heat map depicts expression patterns of 76 metabolism-related genes curated from the literature, of which 61 were significantly altered in AS patients, with the majority being downregulated. Red indicates that a sample has higher than average expression for a given gene while green indicates lower than average expression. Transcriptomic data are based on 17 individuals with severe AS undergoing aortic valve replacement (AVR) in comparison with 13 control subjects (patients with coronary artery disease, normal LV systolic function, and no significant aortic valve disease). Metabolomic data are based on 38 individuals in the control group and 36 in the aortic stenosis group.



circuitry of AS patients, in particular downregulation of multiple components of FA metabolism (Figure 6).

### 3.5 | Modeling increases in acyl-carnitines and their impact on $\beta$ -oxidation

Van Eunen and colleagues<sup>36</sup> developed a number of models for  $\beta$ -oxidation within the systems modeling software package COPASI (<http://copasi.org/>) for both the mouse and humans. While parameters were based on liver tissue, we used the model for human  $\beta$ -oxidation using competition. We initially modeled the impact of increasing cytosolic concentrations of palmitoyl (C16:0)-CoA ranging from 20 to 300  $\mu$ M on flux through  $\beta$ -oxidation as measured by oxidation of NADH and FADH<sub>2</sub>. Initially, flux increased up to 80  $\mu$ M of palmitoyl-CoA and then flux decreased by 5% (Figure 7A). We then examined how tissue concentrations of C14:0-carnitine might inhibit  $\beta$ -oxidation. Increasing concentrations of mitochondrial C14:0-carnitine from 1 to 50  $\mu$ M inhibited  $\beta$ -oxidation under conditions where the model used either 20 or 50  $\mu$ M of palmitoyl-CoA (Figure 7B,C). Thus, accumulation of mid- and long-chain acyl-carnitines may inhibit oxidation as a result of increasing concentrations of mid- and long-chain acyl-CoAs which in turn are competitive inhibitors of acyl-CoA dehydrogenases.

## 4 | DISCUSSION

Here, we leveraged a targeted metabolomic approach in well-defined human cohorts to draw biological insights into two common etiologies of LVH: AS and HCM. Our systems medicine approaches disclosed a concordant bio-signature for reduced FAO in AS which, in the case of the plasma metabolome, was distinct from HCM in terms of magnitude.

Using a similar multi-site sampling approach to that recently described,<sup>46</sup> we observe that predictive models to discriminate between AS, HCM, and control populations performed best using samples obtained centrally (AR/CS) rather than peripherally (FV). However, the absolute reductions in AUCs were relatively small, enabling confirmation of the model from peripheral blood in a separate validation cohort.

By withdrawing paired blood samples from the AR and CS, we were able to directly examine transmyocardial metabolite gradients in vivo in human.<sup>47</sup> We found that the heart is a net importer of glutamate, 2-oxo-isovalerate, 2-oxo-3-methylvalerate,

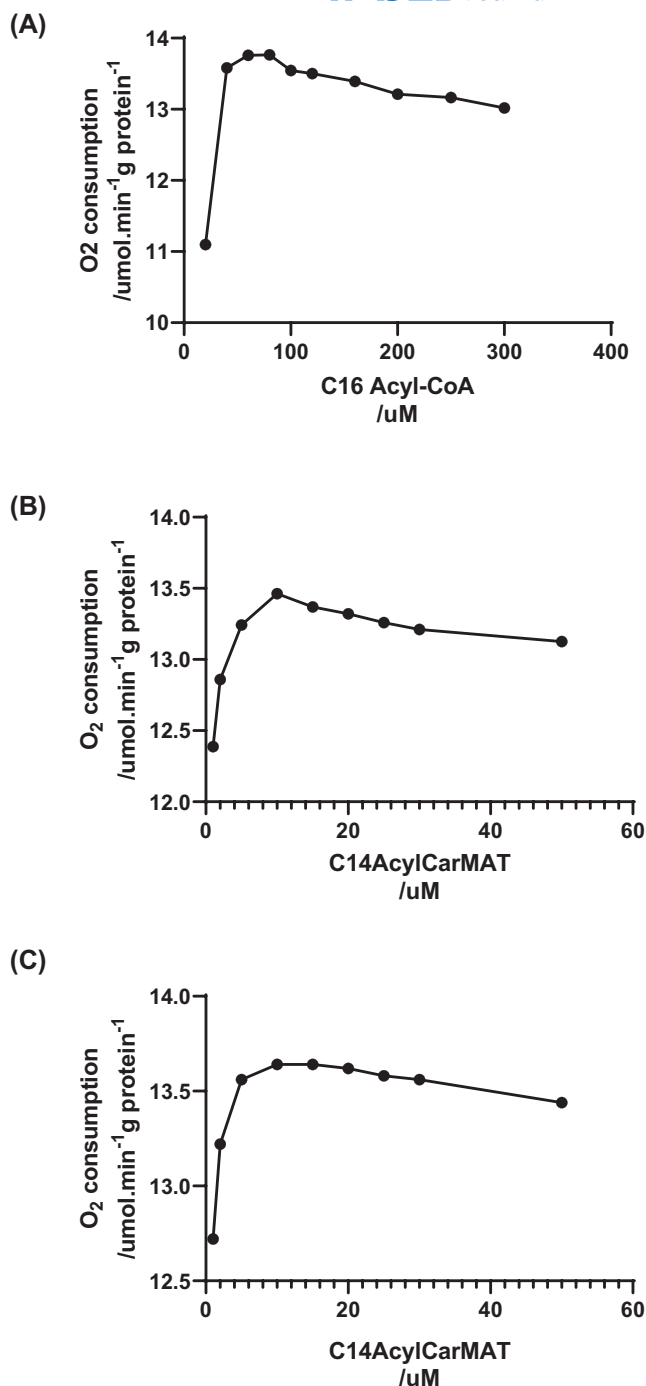


**FIGURE 7** Modeling of  $\beta$ -oxidation to investigate the potential impact of long-chain fatty acids on flux. A model of competitive inhibition in human metabolism based on the model by van Eunen and colleagues<sup>36</sup> was used to investigate the impact of varying concentrations of either palmitoyl-CoA or C14:0-carnitine on  $\beta$ -oxidation. (A) Modeling of flux variation as measured by O<sub>2</sub> consumption for the oxidation of NADH and FADH<sub>2</sub> generated against varying concentrations of palmitoyl-CoA. (B) Modeling of flux variation under constant concentration of 20  $\mu$ M palmitoyl-CoA with varying concentrations of C14:0-carnitine. (C) Modeling of flux variation under constant concentration of 50  $\mu$ M palmitoyl-CoA with varying concentrations of C14:0-carnitine.

2-oxo-isocaproate, and pyruvate, while it elutes succinate, malate, and 3-hydroxybutyrate. The import of glutamate and metabolites of branch chain amino acids indicate that the heart undergoes significant anaplerosis in order to maintain the citric acid cycle. Lahey and colleagues have previously reported increased malic enzyme I expression in hypertrophic rats induced by transverse aortic constriction and patients with heart failure.<sup>48</sup> Malic enzyme produces malate through the carboxylation of pyruvate and was shown to reduce cellular concentrations of NADPH and reduced glutathione production.

Contrasting with recent studies highlighting a role for increased myocardial ketone body consumption as an alternative substrate to FAO in human and rodent failing hearts,<sup>49</sup> we observed a net elution of  $\beta$ -hydroxybutyrate across control, AS, and HCM groups. Bedi and colleagues<sup>49</sup> compared biopsies from end-stage human failing hearts at the time of orthotopic transplantation or LV assist device implantation with non-failing hearts from brain-dead organ donors. They reported reductions in both cardiac lipid species and expression of enzymes involved in lipid metabolism including mid- and long-chain acylcarnitines, the high-affinity carnitine transporter (*SLC22A5*),<sup>49</sup> but upregulation in  $\beta$ -hydroxybutyrate dehydrogenase 1 and 2 (*BDH1* and *BDH2*) in end-stage HF, but not non-failing hearts (including those with LVH). Using mitochondrial proteomic profiling, Aubert and co-workers reported similar upregulation changes in murine models of both compensated LVH and HF, together with downregulation in enzymes involved in FAO, and a marked increase in *BDH1* along with flux measurements consistent with increased oxidation of ketone bodies.<sup>50</sup> Thus, the heart expresses the enzymes for producing ketone bodies. Combined with our findings, these data allude to specificity of metabolic rewiring in LVH versus advanced HF, and in AS there is a reduction in the oxidation of  $\beta$ -hydroxybutyrate that leads to its export from the heart. However, this result was in contrast to those described by Voros and colleagues who described increased uptake of ketone bodies in patients with AS and Heart Failure with Reduced Ejection Fraction (HFrEF),<sup>51</sup> suggesting whether the heart exports or imports ketone bodies depends on the stage of the disease.

Somewhat surprisingly, as compared to individual collection sites, the trans-myocardial gradients had a poor discriminatory power for disease state. However, we were unable to measure coronary sinus flow in this study, in part because it was so variable in the AS group. Differences in flow between the study groups could be a confounder in measuring trans-myocardial gradients. Predictive models could be built by examining samples from the CS, AR, and FV that readily discriminated AS from the two other cohorts. This suggests that the

classification models rely, in part, on systemic metabolism changes as much as those directly from the heart, suggesting that AS and HCM should be understood as systemic disease processes.<sup>52</sup>

Individuals with AS constituted the group most readily discriminated from normal subjects by plasma metabolomic profile. This was largely characterized by increases in long-chain acylcarnitine moieties, including C14, C16:1, and C18-OH, a metabolic signature suggesting incomplete FAO downstream of CPT-1, resonating with observations in advanced human HF.<sup>49</sup> These long-chain acylcarnitine species are independently associated with maladaptive LV remodeling in patients with severe symptomatic AS.<sup>53</sup> Similarly, our transcriptomic evaluation of LV biopsies from patients with AS highlighted the most prominent gene expression changes to affect lipid metabolism. Notably, this included downregulation in specific components of mitochondrial  $\beta$ -oxidation, recently implicated as a likely contributor to the global acylcarnitine profile of severe HF.<sup>54</sup> We further identified downregulation in cardiac-enriched subunit isoforms of the heterotrimeric master cellular energy gauge, AMPK, a key promoter of FA catabolism. AMPK's actions include phosphorylation of the cytosolic enzyme acetyl-CoA carboxylase (ACC), reducing malonyl-CoA, thereby decreasing both the substrate for FA synthesis and simultaneously de-repressing CPT-1 activity to promote long-chain fatty acyl-CoA mitochondrial influx, in addition to influencing energy homeostasis and mitochondrial biogenesis via *ERR $\alpha$*  and *PGC1- $\alpha$* .<sup>55</sup>

Our finding of a large number of metabolic genes whose expression changes in AS, alludes to a significant cardiac metabolic reconfiguration in pressure overload-induced LVH, an observation mirrored in murine HF models<sup>56</sup> and potentially including altered mitochondrial protein acetylation, shown to involve FAO enzymes in HF.<sup>57</sup> In agreement with our study, previous studies of HF have described increased long-chain acyl-carnitines in end-stage HF<sup>58,59</sup> and pressure-overload induced HF,<sup>60</sup> with these increases being reduced when patients are placed on circulatory support.<sup>59</sup> Turer and co-workers employed paired-blood sampling to calculate that, following ischemia-reperfusion, patients with left ventricular systolic dysfunction (LVSD) have reduced FFA uptake from the blood compared to controls.<sup>41</sup> Yang and colleagues and Qiu and co-workers using the coronary artery ligation, MI induced-HF rat model, inferred alterations in FA biosynthesis and elongation from urinary metabolites, and noted an increase in long-chain FAs in the blood, respectively.<sup>61,62</sup> Conversely, Lai and colleagues noted an increase in myocardial long-chain acyl-carnitine species and a decrease in L-carnitine in mice with HF.<sup>56</sup> This may reflect differences in the staging of HF across patients and different model systems. It should be noted though that the

microarray study in this manuscript was modest in size, making it impossible to explore how further confounding variables (e.g., age, sex) impact the dataset we produced, although its agreement in terms of affected pathways with our larger metabolomic study is reassuring.

Previously, van Eunen and colleagues have developed a model of  $\beta$ -oxidation in mouse and human liver, although using a number of parameters taken from the heart.<sup>36,37</sup> They observed that substrate competition for acyl-CoA dehydrogenases led to inhibition of the pathway. We used the human model with competition to investigate whether medium/long-chain carnitines could inhibit  $\beta$ -oxidation in the heart. Using the model to investigate increasing fatty acid oxidation by raising the concentration of cytosolic palmitoyl-CoA, we recapitulated the previous observation that substrate inhibition reduced  $\beta$ -oxidation at higher substrate concentrations. We next simulated an increase in a medium-chain carnitines in the mitochondria. While low concentrations of C14:0-carnitine in the mitochondria stimulated flux through the pathway as measured by the rate of oxidation of NADH and FADH<sub>2</sub>, at concentrations above 15  $\mu$ M there was a progressive inhibition. The impact of substrate inhibition could be even greater in the failing heart. In the model, oxygen consumption was allowed to rise with increase in flux but in patients with HF, the capacity to increase flux through the electron transport chain is likely to be limited further exasperating the accumulation of long and medium-chain acyl-carnitines.

The current study has a number of potential limitations and caveats. Transcardiac metabolite gradient variability, especially with pacing, is not completely indicative of extent of associated changes in myocardial metabolism, because coronary sinus flow was not measured. Arterial-venous concentration differences are dependent on blood flow and as coronary sinus flow was not measured in this study, the differences in flow between the study groups could be a major confounder. However, much of the analyses in the manuscript focus on steady-state concentrations as ‘snap-shots’ of metabolism and these performed better in terms of disease classification, possibly because of the confounding factor of sinus blood flow for the transcardiac measurements. The basis for accumulation of acylcarnitines in AS could represent, in part, saturation of capacity of CPT2, which functions to dissociate long-chain fatty acids from carnitine on inner mitochondrial membranes. The AS group in the first cohort was also significantly older and had a higher proportion of women. To address this, we performed further multivariate analyses on a sub-set of samples from patients over 70 and verified this older group produced similar models to the whole cohort. Similarly, analyses of only males produced similar results to the entire cohort indicating the original multivariate models were not biased according to sex. Finally,

the “control” subjects used for obtaining myocardial biopsies were undergoing surgery for symptomatic coronary disease, and had mild LVH; thus, this group cannot be entirely regarded as true “controls”.

In summary, we identify substantial differences in the plasma metabolic profiles accompanying two canonical forms of LVH, specifically that an acylcarnitine accumulation bio-signature indicative of repressed FAO is associated strongly with human LV pressure overload represented by AS, supported by the finding of transcriptome reprogramming of FA metabolism. Our findings have important implications for attempts at metabolic modulation of LVH and the transition to HF, including in AS where, even in the setting of contemporary surgical or percutaneous valve replacement, myocardial remodeling,<sup>28,63</sup> and dysfunction<sup>64</sup> powerfully predict prognosis.

### AUTHOR CONTRIBUTIONS

Nikhil Pal, Animesh Acharjee, Zsuzsanna Ament, Hugh Watkins, Houman Ashrafian, and Julian L. Griffin designed the main study and wrote the manuscript. Zsuzsanna Ament, James West, and William Briggs performed the metabolomics analysis. Animesh Acharjee and Julian L. Griffin performed multivariate statistics on the metabolomic data. Houman Ashrafian, Violetta Steeples, Helen Lockstone, and Kate Elliott performed transcriptional analysis on cardiac tissue. All authors read and approved the final manuscript. Nikhil Pal, Animesh Acharjee, and Zsuzsanna Ament share the first author position to reflect the fact that they led the human intervention study (Nikhil Pal), the metabolomic analysis (Zsuzsanna Ament), and the bioinformatics (Animesh Acharjee).

### ACKNOWLEDGMENTS

The research was supported by grants MR/P011705/1, MC\_UP\_A090\_1006, and MR/P01836X/1. HA HW, and NP are supported by the University of Oxford Biomedical Research Centre, NIHR.

### DISCLOSURES


The authors declare no conflicts of interest.

### DATA AVAILABILITY STATEMENT

The metabolomic data from this publication are freely available from the MetaboLights repository.

### ORCID

Animesh Acharjee  <https://orcid.org/0000-0003-2735-7010>

Zsuzsanna Ament  <https://orcid.org/0000-0002-0316-4348>

Houman Ashrafian  <https://orcid.org/0000-0003-3988-378X>

Houman Ashrafian  <https://orcid.org/0000-0003-3988-378X>

Julian L. Griffin  <https://orcid.org/0000-0003-1336-7744>

## REFERENCES

- Lopaschuk GD, Ussher JR, Folmes CD, Jaswal JS, Stanley WC. Myocardial fatty acid metabolism in health and disease. *Physiol Rev.* 2010;90(1):207-258.
- Neubauer S, Horn M, Pabst T, et al. Cardiac high-energy phosphate metabolism in patients with aortic valve disease assessed by 31P-magnetic resonance spectroscopy. *J Investig Med.* 1997;45(8):453-462.
- Shen W, Asai K, Uechi M, et al. Progressive loss of myocardial ATP due to a loss of total purines during the development of heart failure in dogs: a compensatory role for the parallel loss of creatine. *Circulation.* 1999;100(20):2113-2118.
- Neubauer S, Horn M, Cramer M, et al. Myocardial phosphocreatine-to-ATP ratio is a predictor of mortality in patients with dilated cardiomyopathy. *Circulation.* 1997;96(7):2190-2196.
- Neubauer S. The failing heart—an engine out of fuel. *N Engl J Med.* 2007;356(11):1140-1151.
- Doenst T, Nguyen TD, Abel ED. Cardiac metabolism in heart failure: implications beyond ATP production. *Circ Res.* 2013;113(6):709-724.
- Dávila-Román V, Vedala G, Herrero P, et al. Altered myocardial fatty acid and glucose metabolism in idiopathic dilated cardiomyopathy. *J Am Coll Cardiol.* 2002;40(2):271-277.
- Osorio JC, Stanley WC, Linke A, et al. Impaired myocardial fatty acid oxidation and reduced protein expression of retinoid X receptor-alpha in pacing-induced heart failure. *Circulation.* 2002;106(5):606-612.
- De Jong KA, Lopaschuk GD. Complex energy metabolic changes in heart failure with preserved ejection fraction and heart failure with reduced ejection fraction. *Can J Cardiol.* 2017;33(7):860-871.
- Sharov VG, Todor AV, Silverman N, Goldstein S, Sabbah HN. Abnormal mitochondrial respiration in failed human myocardium. *J Mol Cell Cardiol.* 2000;32(12):2361-2367.
- Weiss RG, Gerstenblith G, Bottomley PA. ATP flux through creatine kinase in the normal, stressed, and failing human heart. *Proc Natl Acad Sci U S A.* 2005;102(3):808-813.
- Neglia D, De Caterina A, Marraccini P, et al. Impaired myocardial metabolic reserve and substrate selection flexibility during stress in patients with idiopathic dilated cardiomyopathy. *Am J Physiol Heart Circ Physiol.* 2007;293(6):H3270-H3278.
- Barger PM, Brandt JM, Leone TC, Weinheimer CJ, Kelly DP. Deactivation of peroxisome proliferator-activated receptor-alpha during cardiac hypertrophic growth. *J Clin Invest.* 2000;105(12):1723-1730.
- Oka S, Zhai P, Yamamoto T, et al. Peroxisome proliferator activated receptor-alpha Association with silent information regulator 1 suppresses cardiac fatty acid metabolism in the failing heart. *Circ Heart Fail.* 2015;8(6):1123-1132.
- Sihag S, Cresci S, Li AY, Sucharov CC, Lehman JJ. PGC-1alpha and ERRalpha target gene downregulation is a signature of the failing human heart. *J Mol Cell Cardiol.* 2009;46(2):201-212.
- Korvald C, Elvenes OP, Myrnes T. Myocardial substrate metabolism influences left ventricular energetics in vivo. *Am J Physiol Heart Circ Physiol.* 2000;278(4):H1345-H1351.
- Zhang L, Jaswal JS, Ussher JR, et al. Cardiac insulin-resistance and decreased mitochondrial energy production precede the development of systolic heart failure after pressure-overload hypertrophy. *Circ Heart Fail.* 2013;6(5):1039-1048.
- Byrne NJ, Levesseur J, Sung MM, et al. Normalization of cardiac substrate utilization and left ventricular hypertrophy precede functional recovery in heart failure regression. *Cardiovasc Res.* 2016;110(2):249-257.
- Abozguia K, Elliott P, McKenna W, et al. Metabolic modulator perhexiline corrects energy deficiency and improves exercise capacity in symptomatic hypertrophic cardiomyopathy. *Circulation.* 2010;122(16):1562-1569.
- Schmidt-Schweda S, Holubarsch C. First clinical trial with etomoxir in patients with chronic congestive heart failure. *Clinical Sci.* 2000;99(1):27-35.
- Fragasso G, Perseghin G, De Cobelli F, et al. Effects of metabolic modulation by trimetazidine on left ventricular function and phosphocreatine/adenosine triphosphate ratio in patients with heart failure. *Eur Heart J.* 2006;27(8):942-948.
- Heusch G, Libby P, Gersh B, et al. Cardiovascular remodeling in coronary artery disease and heart failure. *Lancet.* 2014;383(9932):1933-1943.
- Grossman W, Jones D, McLaurin LP. Wall stress and patterns of hypertrophy in the human left ventricle. *J Clin Invest.* 1975;56(1):56-64.
- Zhang J, Merkle H, Hendrich K, et al. Bioenergetic abnormalities associated with severe left ventricular hypertrophy. *J Clin Invest.* 1993;92(2):993-1003.
- Levy D, Garrison RJ, Savage DD, Kannel WB, Castelli WP. Prognostic implications of echocardiographically determined left ventricular mass in the Framingham Heart Study. *N Engl J Med.* 1990;322(22):1561-1566.
- de Simone G, Gottdiener JS, Chinali M, Maurer MS. Left ventricular mass predicts heart failure not related to previous myocardial infarction: the Cardiovascular Health Study. *Eur Heart J.* 2008;29(6):741-747.
- Spirito P, Bellone P, Harris KM, Bernabo P, Bruzzi P, Maron BJ. Magnitude of left ventricular hypertrophy and risk of sudden death in hypertrophic cardiomyopathy. *N Engl J Med.* 2000;342(24):1778-1785.
- Cioffi G, Faggiano P, Vizzardi E, et al. Prognostic effect of inappropriately high left ventricular mass in asymptomatic severe aortic stenosis. *Heart.* 2011;97(4):301-307.
- Devereux RB, Wachtell K, Gerds E, et al. Prognostic significance of left ventricular mass change during treatment of hypertension. *JAMA.* 2004;292(19):2350-2356.
- Garg S, de Lemos JA, Ayers C, et al. Association of a 4-tiered classification of LV hypertrophy with adverse CV outcomes in the general population. *J Am Coll Cardiol Img.* 2015;8(9):1034-1041.
- Griffin JL, Atherton H, Shockcor J, Atzori L. Metabolomics as a tool for cardiac research. *Nat Rev Cardiol.* 2011;8(11):630-643.
- West JA, Beqqali A, Ament Z, et al. A targeted metabolomics assay for cardiac metabolism and demonstration using a mouse model of dilated cardiomyopathy. *Metabolomics.* 2016;12:59.
- Roberts LD, West JA, Vidal-Puig A, Griffin JL. Methods for performing Lipidomics in white adipose tissue. *Methods Enzymol.* 2014;538:211-231.
- Diaz-Urriarte R, De Andres SA. Gene selection and classification of microarray data using random forest. *BMC Bioinform.* 2006;7(1):3.



35. Gentleman RCV, Huber W, Irizarry R, Dudoit S. *Bioinformatics and Computational Biology Solutions Using R and Bioconductor*. Springer-Verlag; 2005.
36. van Eunen K, Simons SMJ, Gerding A, et al. Biochemical competition makes fatty-acid b-oxidation vulnerable to substrate overload. *PLoS Comput Biol*. 2013;9(8):e1003186.
37. van Eunen K, Volker-Touw CML, Gerding A, et al. Living on the edge: substrate competition explains loss of robustness in mitochondrial fatty-acid oxidation disorders. *BMC Biol*. 2016;14:107.
38. Johnson BD, Shaw LJ, Pepine CJ, et al. Persistent chest pain predicts cardiovascular events in women without obstructive coronary artery disease: results from the NIH-NHLBI-sponsored Women's Ischaemia Syndrome Evaluation (WISE) study. *European Heart J*. 2006;27(12):1408-1415.
39. Bugiardini R. Women, 'non-specific' chest pain, and normal or near-normal coronary angiograms are not synonymous with favourable outcome. *European Heart J*. 2006;27:1387-1389.
40. Makrecka M, Kuka J, Volska K, et al. Long-chain acylcarnitine content determines the pattern of energy metabolism in cardiac mitochondria. *Mol Cell Biochem*. 2014;395(1-2):1-10.
41. Turer AT, Stevens RD, Bain JR, et al. Metabolomic profiling reveals distinct patterns of myocardial substrate use in humans with coronary artery disease or left ventricular dysfunction during surgical ischemia/reperfusion. *Circulation*. 2009;119(13):1736-1746.
42. Thomassen A, Bagger JP, Nielsen TT, Henningsen P. Altered global myocardial substrate preference at rest and during pacing in coronary artery disease with stable angina pectoris. *Am J Cardiol*. 1988;62(10 Pt 1):686-693.
43. Roberts LD, Bostrom P, O'Sullivan JF, et al. Beta-Aminoisobutyric acid induces browning of white fat and hepatic beta-oxidation and is inversely correlated with cardiometabolic risk factors. *Cell Metab*. 2014;19(1):96-108.
44. Gentleman R, Carey V, and Huber W. *Bioinformatics and Computational Biology Solutions Using R and Bioconductor*. New York: Springer-Verlag; 2006.
45. Zhang P, Hu X, Xu X, et al. AMP activated protein kinase-alpha2 deficiency exacerbates pressure-overload-induced left ventricular hypertrophy and dysfunction in mice. *Hypertension*. 2008;52(5):918-924.
46. Lewis GD, Wei R, Liu E, et al. Metabolite profiling of blood from individuals undergoing planned myocardial infarction reveals early markers of myocardial injury. *J Clin Invest*. 2008;118:3503-3512.
47. Taegtmeier H, Young ME, Lopaschuk GD, et al. Assessing cardiac metabolism: a scientific statement from the American Heart Association. *Circ Res*. 2016;118(10):1659-1701.
48. Lahey R, Carley AN, Wang X, et al. Enhanced redox state and efficiency of glucose oxidation with miR based suppression of maladaptive NADPH-dependent malic enzyme 1 expression in hypertrophied hearts. *Circ Res*. 2018;122(6):836-845.
49. Bedi KC SN Jr, Brandimarto J, Aziz M, et al. Evidence for intramyocardial disruption of lipid metabolism and increased myocardial ketone utilization in advanced human heart failure. *Circulation*. 2016;133(8):706-716.
50. Aubert GMO, Horton JL, Lai L, et al. The failing heart relies on ketone bodies as a fuel. *Circulation*. 2016;133(8):698-705.
51. Voros G, Ector J, Garweg C, et al. Increased cardiac uptake of ketone bodies and free fatty acids in human heart failure and hypertrophic left ventricular remodeling. *Circ Heart Fail*. 2018;11(12):e004953.
52. Otto CM, Prendergast B. Aortic-valve stenosis—from patients at risk to severe valve obstruction. *NEnglJMed*. 2014;371(8):744-756.
53. Elmariah S, Farrell LA, Furman D, et al. Association of acylcarnitines with left ventricular remodeling in patients with severe aortic stenosis undergoing transcatheter aortic valve replacement. *JAMA Cardiol*. 2018;3(3):242-246.
54. Ruiz M, Labarthe F, Fortier A, et al. Circulating acylcarnitine profile in human heart failure: a surrogate of fatty acid metabolic dysregulation in mitochondria and beyond. *Am J Physiol Heart Circ Physiol*. 2017;313(4):H768-H781.
55. Hu X, Xu X, Lu Z, et al. AMP activated protein kinase-alpha2 regulates expression of estrogen-related receptor-alpha, a metabolic transcription factor related to heart failure development. *Hypertension*. 2011;58(4):696-703.
56. Lai L, Leone TC, Keller MP, et al. Energy metabolic reprogramming in the hypertrophied and early stage failing heart: a multisystems approach. *Circ Heart Fail*. 2014;7(6):1022-1031.
57. Horton JL, Martin OJ, Lai L, et al. Mitochondrial protein hyperacetylation in the failing heart. *JCI Insight*. 2016;2(1):e84897.
58. Cheng ML, Wang CH, Shiao MS, et al. Metabolic disturbances identified in plasma are associated with outcomes in patients with heart failure: diagnostic and prognostic value of metabolomics. *J Am Coll Cardiol*. 2015;65(15):1509-1520.
59. Ahmad T, Kelly JP, McGarrah RW, et al. Prognostic implications of long-chain Acylcarnitines in heart failure and reversibility with mechanical circulatory support. *J Am Coll Cardiol*. 2016;67(3):291-299.
60. Sansbury BE, DeMartino AM, Xie Z, et al. Metabolomic analysis of pressure-overloaded and infarcted mouse hearts. *Circ Heart Fail*. 2014;7(4):634-642.
61. Yang D, Wang X, Wu Y, et al. Urinary metabolomic profiling reveals the effect of Shenfu decoction on chronic heart failure in rats. *Molecules*. 2015;20(7):11915-11929.
62. Qiu Q, Li C, Wang Y, et al. Plasma metabolomics study on Chinese medicine syndrome evolution of heart failure rats caused by LAD ligation. *BMC Complement Altern Med*. 2014;14:232.
63. Duncan AI, Lowe BS, Garcia MJ, et al. Influence of concentric left ventricular remodeling on early mortality after aortic valve replacement. *Ann Thorac Surg*. 2008;85(6):2030-2039.
64. Dahl JS, Videbaek L, Poulsen MK, Rudbaek TR, Pellikka PA, Moller JE. Global strain in severe aortic valve stenosis: relation to clinical outcome after aortic valve replacement. *Circ Cardiovasc Imaging*. 2012;5(5):613-620.

## SUPPORTING INFORMATION

Additional supporting information can be found online in the Supporting Information section at the end of this article.

**How to cite this article:** Pal N, Acharjee A, Ament Z, et al. Metabolic profiling of aortic stenosis and hypertrophic cardiomyopathy identifies mechanistic contrasts in substrate utilization. *The FASEB Journal*. 2024;38:e23505. doi:[10.1096/fj.202301710RR](https://doi.org/10.1096/fj.202301710RR)